IOPscience iopscience.iop.org

Home Search Collections Journals About Contact us My IOPscience

Two-level model of oscillating electric-field-induced current instability and chaos in n-GaAs

This article has been downloaded from IOPscience. Please scroll down to see the full text article.

2007 J. Phys.: Condens. Matter 19 116208

(http://iopscience.iop.org/0953-8984/19/11/116208)

View the table of contents for this issue, or go to the journal homepage for more

Download details:
IP Address: 129.252.86.83
The article was downloaded on 28/05/2010 at 16:36

Please note that terms and conditions apply.

IOP PUBLISHING JOURNAL OF PHYSICS: CONDENSED MATTER

J. Phys.: Condens. Matter **19** (2007) 116208 (12pp) doi:10.1088/0953-8984/19/11/116208

Two-level model of oscillating electric-field-induced current instability and chaos in n-GaAs

K Liu[1], **S Y T Tzeng**[2] **and Y Tzeng**[3]

[1] General Education Center, National Taipei University of Technology, Taipei, Taiwan 106, Republic of China
[2] Department of Electro-Optical Engineering, National Taipei University of Technology, Taipei, Taiwan 106, Republic of China
[3] Institute of Physics, Academia Sinica, Taipei, Taiwan 115, Republic of China

E-mail: sytsay@ntut.edu.tw

Received 6 December 2006, in final form 25 January 2007
Published 5 March 2007
Online at stacks.iop.org/JPhysCM/19/116208

Abstract
The authors extend the well accepted two-impurity-level model by including the time-dependent balance equation of the mean electron energy to illustrate the current instability for an n-GaAs semiconductor device with planar-type contacts when an ac bias $E_{\mathrm{ac}}\sin(2\pi f_{\mathrm{d}}t)$ is added to the applied dc bias E_0. To avoid any complications arising from photo-excitation, the authors consider the device in the dark condition. The authors inspect the instability patterns either by keeping the magnitude of dc bias and the frequency of ac current fixed but varying the amplitude of ac bias or by fixing the amplitude and the frequency of ac bias but changing the dc bias. The results of numerical simulations are demonstrated in detail and the system's bifurcating to chaos via several period-doubling routes can be clearly seen in both cases. The bifurcation maps described as a function of the ac drive amplitude E_{ac} or the dc electric field across the sample E_{dc} preserve the main features of the experimental observations by Aoki (1992 *Semicond. Sci. Technol.* **7** B474) and Aoki and Yamamoto (1989 *Appl. Phys.* A **48** 111).

1. Introduction

Transport instabilities in a semiconductor can be well characterized by a nonlinear dependence of the current density J upon the electric field E. This relation is often non-monotonic and displays negative differential conductivity (NDC), which leads to an N-shaped or an S-shaped $J(E)$ characteristic. In general, devices operated in the NDC region are often unstable against temporal or spatial fluctuations of carrier current density. Examining these instabilities can improve our understanding of the performances of semiconductor devices.

There exist quite a few experimental and theoretical works on this subject for different types of semiconductors. For example, instabilities observed and studied in high purity

© 2007 IOP Publishing Ltd Printed in the UK

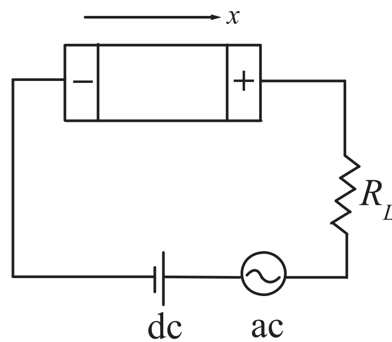

Figure 1. The circuit equivalent to the experimental semiconductor device with the planar-type contacts.

n-GaAs at 4.2 K include the driven chaos induced by periodically modulated bias voltage [1–4], that by weak perpendicular and/or longitudinal magnetic fields [5–13], and the self-generated chaos which is observed under dc conditions and is broadly independent of external conditions [14–24]. We have discussed the magnetic effects in our previous works [25–27]. In this work, we will concentrate on the instability and chaos driven by an oscillating voltage.

Early in 1983, Teitsworth *et al* [28] reported the experimental discovery of subharmonic and chaotic behaviours in periodically driven extrinsic Ge photoconductors. The observations were qualitatively interpreted by a theoretical spatially uniform rate-equation model with a time-dependent current produced by modulated far-infrared (FIR) illumination [29]. Also, Aoki *et al* have investigated periodically driven oscillatory instabilities on n-GaAs [1–4]. Under the so called dark condition (for which external light is completely shielded) at 4.2 K, the I–V curve of the n-GaAs exhibits a dc stable hysteresis. The nonlinear response of a periodically driven current instability has been investigated by applying a dc + ac bias. With the amplitudes larger than the hysteresis width, they observed various types of frequency locking and chaos when the load line was biased in the hysteresis region [2–4]. The period-doubling bifurcations were found by varying either the magnitude of the dc bias or that of ac bias. They employed a phenomenological one-level impact-ionization model [30–32] to study these findings theoretically. In an alternative way, we would like to adopt Scholl's two-impurity-level model, with the assumption of spatial homogeneity, to discuss the driven instability phenomena at helium temperatures.

Our computer simulation for the experimental equivalent circuit shown in figure 1 with ac bias will be briefly described in section 2. Because Schöll's two-level model can capture the essential features of SNDC well, we adopt this model to examine ac driven instability. The governing dynamic equations are basically the same as the previous model. For a more accurate description of the SNDC model, we employ the field-dependent and density-dependent electron mobility and furthermore write it in the phenomenological form. We also adopt the energy balance equation, and take into account the temperature dependence of the generation–recombination (GR) coefficients. This is because the presence of impurities plays a crucial role in causing SNDC. At helium temperature the binding energies of the impurities for free carriers are larger than their thermal energy. Thus, all of the carriers tend to be trapped by the impurities. Although thermal ionization of the electrons in the impurity sites to the conduction band is not possible, the trapped electrons can be ionized to the conduction band by the accelerated free electrons that are driven by an external electric field (called impact ionization). Therefore, the free carriers may be captured by the ionized impurity sites or be generated through the impact

ionization upon the trapped electrons. Based on the above arguments, the transport properties of semiconductors are seriously affected by the generation and recombination of the free carriers between the conduction band and the impurity levels. The impact ionization coefficients X_1 and X_1^* as well as the capture coefficient T_1^S have been calculated from Monte Carlo simulation by Scholl's group [33, 34] and furthermore expressed in terms of the electron temperatures and carrier density by fit functions. For the impact ionization coefficients we basically adopt the lucky-electron model [35] and express the dependence of the impact ionization coefficients upon the electron density and electric field through the electron temperatures and electric field. For the capture coefficient T_1^S, a form similar to that in [34] has been used to reflect the enhancement characteristic near the breakdown field where the low frequency oscillations are expected.

Since the current filament is dc unstable under weak photo-excitation, to avoid further complications, here we consider the device at the dark condition so that the oscillatory behaviour under photo-excitation can be ignored. Based on the theoretical formulation, the numerical simulations are performed. We either keep the magnitude of the dc bias and the ac frequency constant but vary the amplitude of the ac bias, or fix the amplitude and the frequency of the ac bias but alter the dc bias to examine the instabilities. From our simulations under these two circumstances, we do obtain oscillatory instabilities bifurcating to chaos, as will be displayed in section 3 in detail. Simulation results presented here in phase portraits, in power spectra, and in bifurcation maps show a period doubling cascade to chaotic oscillation for increasing sinusoidal drive amplitude E_{ac} and dc bias E_0.

2. Model

In the two-impurity-level model for n-GaAs, the carrier density n in the conduction band is governed by the generation–recombination (GR) process in which an electron in the ground or the first excited state of the impurity may be thermally or impact ionized to the conduction band and may then recombine with a donor having an empty state [14, 36]. The electron density n in the conduction band, the ground level density n_{t_1} and the first excited level density n_{t_2} can be expressed through the GR rate equations

$$\dot{\nu} = \phi(\nu, \nu_{t_1}, \nu_{t_2}, E) \tag{1}$$

$$\dot{\nu}_{t_i} = \phi_{t_i}(\nu, \nu_{t_1}, \nu_{t_2}, E), \qquad i = 1, 2 \tag{2}$$

with $\nu = n/N_D^*, \ldots$, etc, $N_D^* = N_D - N_A$ being the effective doping concentration, N_D, N_A the donor and the acceptor concentrations respectively, E the electric field, and the dot denoting the time derivative. The rate functions ϕ and ϕ_{t_1} can be written as [14, 37]

$$\phi(\nu, \nu_{t_1}, \nu_{t_2}, E) = X_1 N_D^* \nu \nu_{t_1} + (X_1^s + X_1^* N_D^* \nu)\nu_{t_2} - T_1^s N_D^* (N_A/N_D^* + \nu)\nu, \tag{3}$$

$$\phi_{t_1}(\nu, \nu_{t_1}, \nu_{t_2}, E) = -(X^* + X_1 N_D^* \nu)\nu_{t_1} + T^* \nu_{t_2}, \tag{4}$$

with $\nu_{t_2} = 1 - \nu - \nu_{t_1}$ from the conservation of charge. Hence in an explicit GR model for low temperature n-type GaAs, the transition rates ϕ, ϕ_{t_1}, and ϕ_{t_2} between the levels must satisfy $\phi + \phi_{t_1} + \phi_{t_2} = 0$. The magnitudes of the GR coefficients at 4.2 K, liquid-helium temperature, are given in table 1. These coefficients may vary with various factors, such as changes of the electron temperature T_e, applications of external electric field, and so on.

Let us consider the experimental equivalent circuit shown in figure 1 where a static and an ac oscillating electric field are applied in the x direction, $\mathbf{E_s} = (E_0 + E_{ac}\sin(2\pi f_d t))\hat{\mathbf{x}}$. Except this, no magnetic or any other field is present. The ac electric field gives rise to an oscillator impedance Z. Consequently, in the presence of the oscillator the impedance of the equivalent

Table 1. The parameter values corresponding to n-GaAs at 4.2 K for the two-level generation–recombination model studied in this paper.

Parameter	Value
T^*	3.45×10^6 s^{-1}
X_1^{s0}	6.9×10^5 s^{-1}
X^*	1.03×10^6 s^{-1}
X_1^0	6.9×10^{-7} cm^3 s^{-1}
X_1^{*0}	1.38×10^{-5} cm^3 s^{-1}
l	1.0×10^{-3} cm
e_1	6.6×10^{-7} cm^3 s^{-1}
g_1	8.0×10^{-6} cm^3 s^{-1}
(e_2, e_3)	$(2.3, -0.095)$
(g_2, g_3)	$(-0.265, 1.254)$
(ν_{th}, q_1)	$(0.07, 0.693)$
N_A/N_D^*	0.3
r_2	2.3
μ_0	2.5×10^4 cm^2 V^{-1} s^{-1}
v_s	1.25×10^5 cm s^{-1}
T_L	4.2 K
β_0^2	3×10^2
ν_0	5.75×10^{-3}
N_D^*	2.5×10^{14} cm^{-3}
τ_0	6.3×10^{-11} s
$1/\gamma_d$	9.1×10^{-7} s

circuit becomes $Z_{eq} = R_L + Z$ with R_L the load resistance. The dynamical equation for the drift electric field, $\mathbf{E} = E\hat{\mathbf{x}}$, can be written as

$$\dot{E} = -\gamma_d\left(-E_s + E + \frac{AZ_{eq}}{L}J\right) \tag{5}$$

with the current density

$$J = e\nu N_D^* v_d \tag{6}$$

where $1/\gamma_d$ is the effective dielectric relaxation time, and L and A are, respectively, the separation between contacts and the cross-sectional area of the sample. In the above equation, v_d is the drift velocity of the electrons and is generally written as

$$v_d = \mu E. \tag{7}$$

On the lower branch of the S-shaped $n(E)$ characteristic, the velocity is modelled by the empirical saturable form $v_d(E) = v_s \arctan(r_2 E)$ with the saturated drift velocity v_s and the saturation parameter r_2 and the mobility μ_{lo} is written as [19, 38]

$$\begin{aligned}\mu_{lo}(E) &= \frac{v_d(E)}{E}\\ &= v_s\frac{\arctan(r_2 E)}{E}.\end{aligned} \tag{8}$$

On the high conductivity branch of the S-shaped $n(E)$ characteristic, an obvious increase of T_e with rising electric field, scattering is predominant. The electron mobility μ_{up} with density n at temperature T_e is given by the Brooks–Herring (BH) formula [39]

$$\begin{aligned}\mu_{up}(T_e, \nu) &= \mu_{BH}(T_e, \nu)\\ &= \mu_0\left(\frac{T_e}{T_L}\right)^{3/2}\frac{g(\beta_0, \nu_0)}{g(\beta, \nu)},\end{aligned} \tag{9}$$

with

$$g(\beta, \nu) = (2N_A/N_D^* + \nu)(\ln(1+\beta^2) - \beta^2/(1+\beta^2)),$$
$$\beta^2 = \beta_0^2\left(\frac{T_e}{T_L}\right)^2\frac{\nu}{\nu_0},$$

where the dimensionless electron density $\nu_0 = n_0/N_D^*$, and n_0, μ_0, and β_0 are the electron density, the electron mobility, and the so-called BH coefficient, respectively, under zero electric field at T_L. The transition from μ_{lo} to μ_{up} at a certain threshold electron density ν_{th} corresponding to the largest value of ν on the lower branch may be described by saturated drift velocity. Therefore the mobility covering the entire range in ν is represented by

$$\mu(T_e, E, \nu) = \tfrac{1}{2}\{[\mu_{lo}(E) + \mu_{up}(T_e, \nu) + [\mu_{lo}(E) - \mu_{up}(T_e, \nu)]\tanh[(2\log_{10}(\nu_{th}/\nu)]\} \tag{10}$$

For a more accurate description of the two-level model, we consider the energy balance equation. During the GR processes the electron temperature T_e will increase and can be determined through electron mean energy $\mathcal{E} = \frac{3}{2}k_B T_e$, with k_B being the Boltzmann constant. $\mathcal{E}$ is directly related to the electric field E via the energy balance equation [40]

$$\dot{\mathcal{E}} = -(\mathcal{E} - \mathcal{E}_L)/\tau(\mathcal{E}) + e\mu E^2 \tag{11}$$

where $\mathcal{E}_L = \frac{3}{2}k_B T_L$ is the thermal energy at zero electric field with the lattice temperature T_L, and $\tau(\mathcal{E}) \propto \mathcal{E}^{-1/2}$ the energy relaxation time considered theoretically. In line with our previous works [26, 27], equation (11) is also converted to [32]

$$\dot{\bar{T}}_e = -\frac{1}{\tau_0}[\bar{T}_e^{1/2}(\bar{T}_e - 1)] + \frac{2e}{3k_B T_L}\mu E^2 \tag{12}$$

with $\bar{T}_e = T_e/T_L$, and τ_0 the energy relaxation time constant.

On the upper branch, the drift velocity increases obviously as a result of the sharp increase of the electron temperature and density. Since T_e can be determined from the energy balance equation equation (11) or (12) and ν is related to the electric field by GR rate equations (1) and (2), our μ_{BH} in equation (9) used to express the enhancement of the mobility on the upper branch of the $n(E)$ characteristic is dependent on the electric field implicitly. Thus solving the coupled differential equations (1), (2), (5), and (12) enables us to examine the cross-over instability for n-type GaAs due to the effects from the electric field E including the oscillating ac field, our present main interest, and the carrier temperature T_e variation.

An essential part of the two-level model is the generation and recombination of the free carrier between the conduction band and the impurity levels. Besides explicitly appearing in the differential equations, the electron density and electric field may also implicitly be embedded in the GR coefficients. We apply Schöll's group's works [33, 34] to account for the GR coefficients' electric field and electron density dependence, as to be briefly described in the following.

For the impact-ionization coefficients X_1 and X_1^*, basically we adopt the electric field and binding energy dependent lucky-electron model [35]. But as E goes higher than the breakdown field, these X_1 and X_1^* behave differently towards T_e [33]. Since both T_e and X_1 show similar behaviours as E varies [33, 34], a factor $\delta(T_e)$ is multiplied to the cross section of X_1 when the temperature increases,

$$\delta(T_e) = 1 + \lambda T_e/T_L, \tag{13}$$

where λ is an adjustable parameter and is taken to be 0.06. Therefore X_1 becomes

$$X_1(E, T_e) = \delta(T_e)X_1^0 e^{-\varepsilon_b/elE}. \tag{14}$$

On the other hand, because the excited state's ionization energy is much smaller than the ground state's, X_1^* shows a very weak dependence on T_e [33]. Hence we keep X_1^* the same form as that in the lucky-electron model [35],

$$X_1^*(E) = X_1^{*0} e^{-\varepsilon_b^*/elE}, \tag{15}$$

with coefficients X_1^0 and X_1^{*0} and mean free path l being given in table 1, and $\varepsilon_b = 6.0$ and $\varepsilon_b^* = 1.5$ meV the impurity ground and first excited state binding energies for n-GaAs.

Generally, the capture rate decreases monotonically with the field except at the onset of the upper branch, where T_1^s increases because strong impact ionization scatters many carriers back to the band minimum, from where they can recombine with high probability. The capture coefficient T_1^s is represented by [34]

$$\begin{aligned} T_1^s(T_e, \nu) &= \tfrac{4}{5} T_1^{s,\mathrm{lo}}(T_e) + \tfrac{1}{2}\{[T_1^{s,\mathrm{up}}(T_e) + T_1^{s,\mathrm{lo}}(T_e)] + [T_1^{s,\mathrm{up}}(T_e) \\ &\quad - T_1^{s,\mathrm{lo}}(T_e)] \tanh[\log_{10}(\nu/\nu_{\mathrm{th}})^{0.8}]\}, \\ T_1^{s,\mathrm{up}}(T_e) &= e_1 \exp[e_2(T_e/T_L - q_1)^{e_3}], \\ T_1^{s,\mathrm{lo}}(T_e) &= g_1 \exp[g_2(T_e/T_L)^{g_3}] \end{aligned} \tag{16}$$

with parameters $\nu_{\mathrm{th}}, q_1, e_i, g_i, i = 1, \ldots, 3$, being defined in [34].

On the part of the thermal ionization coefficient $X_1^s(T_e)$, we take into account the effect of the Boltzmann factor and write it as

$$X_1^s(T_e) = X_1^{s0} e^{\varepsilon_b^*(1/k_B T_L - 1/k_B T_e)}, \tag{17}$$

where X_1^{s0} is the thermal ionization coefficient at lattice temperature T_L.

3. Simulations and numerical results

We now represent the results of numerical simulations for the two-impurity-level model with the field-dependent and temperature-dependent electron mobility and GR coefficients, to describe the experimental measurements [1–4] performed at 4.2 K under dark conditions for a high purity n-GaAs with a typical rectangular cross-section area $A = 1.8 \times 10^{-4}$ cm^2, and the spacing between the planar-type contacts $L = 2.5$ mm.

We first solve equations (1), (2) and (12) under their stationary state conditions ($\dot{\nu} = \dot{\nu}_{t_1} = \dot{T}_e = 0$), making use of the E- and T_e-dependent GR coefficients mentioned in the previous section. We then obtain the static S-shaped J–E characteristic as shown in figure 2(a). Referring to the reasonable material parameters for n-type GaAs [14, 34], the numerical parameters used in the calculation are tabulated in table 1. As a dc bias voltage V_0 is applied across a series resistance of the GaAs sample and a load resistor R_L, a specified load line is determined by $J = (E_0 - E)/d$, with $d = AR_L/L$, $E_0 = V_0/L$, and $E = V/L$, V being the voltage across the sample. The slope of the load line, $dJ/dE = -1/d$, remains a constant once R_L is specified, but the position of the horizontal intercept varies with the applied field E_0 (or with the dc bias voltage V_0). Hence by setting $R_L = 500\ \Omega$ in our numerical simulations we have the load-line condition as $d = 0.36$ cm V A^{-1}. The load line is biased on the upper branch or lower branch or in the NDC region of the J–E curve, showing no spontaneous relaxation oscillation. The stable hysteresis is formed as shown in figure 2(b) if J is assumed homogeneous over the sample's cross section A.

Steady-state solution of the drift velocity is shown as a function of E in figure 2(c). The drift velocity v_d generally increases with the field E. A strong increase of v_d with rising electric field occurs on the high conductivity branch as opposed to only a slight increase on the low conductivity branch. The remarkable increase in v_d on the upper branch is apparently caused by the screening effect of the ionized impurity scattering in the BH mobility formula (9).

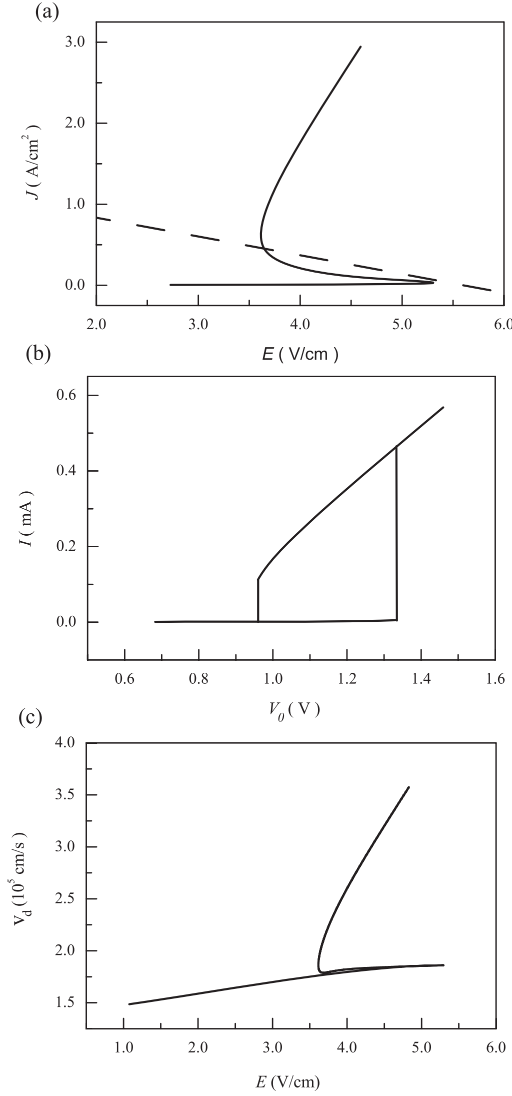

Figure 2. The J–E characteristic (a), the corresponding I–V curve (b) for an S-shaped NDC GaAs, when it is connected in series with a dc bias and a load resistor, and the drift velocity v_d (c). In (a) the dotted line denotes a load line with the load line condition $d^* = AZ_{eq}/L = 4.32$ cm V A^{-1}.

This reveals the same trend as the simulated drift velocity in [33] and keeps a consistent characteristic of the anomalously high mobilities observed inside the current filaments in n-GaAs, as compared to the much lower mobilities outside [41].

Now turn on the ac bias so that the electric field across the GaAs sample and the load resistor R_L is $E_s = E_0 + E_{ac}\sin(2\pi f_d t)$. The impedance of the equivalent circuit Z_{eq} now includes R_L and the oscillator impedance Z. Choosing $Z \sim 5.5$ kΩ, we have $Z_{eq} = 6$ kΩ. Consequently, in the presence of the oscillator (ac bias), the load line becomes $E = E_0 - d^* J$ with the load line condition $d^* = AZ_{eq}/L = 4.32$ cm V A^{-1}. Therefore, we pick up the operating point (E_i, J_i) from the intersection of the J–E characteristic with the load line, as

the dotted line shown in figure 2(a) with the intersection at $E_0 = 5.599\,985$ V cm^{-1} biased in the NDC region of the J–E characteristics. The system is stable without ac bias.

Since the energy relaxation time $\tau_0(\sim 10^{-10}$ s) is shorter than the effective dielectric relaxation time $1/\gamma_d(\sim 1\ \mu$s), the energy balance assumes a quasi-steady state almost instantaneously, determining $\mathcal{E}(T_e)$ as a function of the electric field E, which varies slowly according to equation (5), and the dynamics is dominated by the dielectric field relaxation. By specifying $f_d = 5.5 \times 10^5$ Hz and increasing gradually the magnitude of the amplitude of the ac bias E_{ac} from 0.8 to 0.975 V cm^{-1} when solving equations (1), (2), (5), and (12), we are able to see the period-doubling chaotic bifurcation sequence as shown in figures 3(a)–(e). Plotted in the left column of figures 3(a)–(e) are the phase portraits of the conduction electron concentration ν versus the electric field E for period 1, period 2, period 4, period 8, and chaos with E_{ac} set to be 0.8, 0.9, 0.94, 0.944, and 0.945 V cm^{-1}, respectively. Their corresponding Fourier power spectra of $\nu(t)$ are shown in the right column of figures 3(a)–(e), where a clear peak at $f = f_d$ can be seen from the right part of figure 3(a) for a period-1 limit cycle. Increasing E_{ac} slightly makes it bifurcate to period-2 oscillation with a subharmonic component at $f_d/2$, and then period-4 oscillation with an additional subharmonic component at $f_d/4$, as in figures 3(b) and (c), respectively. At $E_{ac} = 0.944$ V cm^{-1} a period-8 oscillation arises, as in the power spectrum of figure 3(d), and subharmonic components at $f_d/2$, $f_d/4$ and $f_d/8$ can be clearly seen. Finally, chaos appears in figure 3(e) when E_{ac} is raised to or beyond 0.945 V cm^{-1}. The above described behaviours as a function of E_{ac} in the NDC regime are clearly displayed in the bifurcation map as shown in figure 4, where ν_{max} is the maximum value of the electron density for the conduction band. In the map, the oscillations with more periods appear in a shorter interval of E_{ac}, for example, period-2 oscillations existing in 0.885 V cm^{-1} $\leqslant E_{ac} <$ 0.924 V cm^{-1}, period-4 oscillations existing in 0.924 V cm^{-1} $\leqslant E_{ac} <$ 0.943 V cm^{-1}, while period-8 oscillations in a much shorter one, 0.943 V cm^{-1} $\leqslant E_{ac} <$ 0.945 V cm^{-1}. Each figure in figures 3(a)–(e) is a chosen example in each corresponding interval. Beyond the appearance of chaos, further increasing E_{ac} to around 0.967 V cm^{-1}, we also obtain period-5 oscillations. The bifurcation pattern described here is similar to that observed in [3].

To show the rich structure of the bifurcation routes to chaos in the NDC region of the J–E curve and to give a more intuitive understanding, we also choose the dc electric field across the sample E_{dc}, related to the applied static electric field E_0 as $E_{dc} = E_0 - d^* J$, as the control parameter, while E_{ac} and f_d are kept as constants. With an appropriate dc bias E_0 in the NDC branch of the J–E curve, we can find the stable operating point as stated previously, and E_{dc} can thus be determined. In our numerical simulation, we have the magnitude of E_{dc} varied from 3.6375 to 3.6477 V cm^{-1} with the same load-line condition $d^* = 4.32$ cm V A^{-1}. Equations (1), (2), (5), and (12) are now solved by fixing the amplitude E_{ac} at a relatively large value of 0.945 V cm^{-1} and driving frequency at $f_d = 5.5 \times 10^5$ Hz. The results are plotted in figure 5, with ν_{max} being defined in the same way as that in figure 4. In the figure, we can clearly see the de-stability of the period-1 limit cycle via bifurcation to chaos as the control parameter E_{dc} varies. Our bifurcation map shown in figure 5 is similar to the one observed experimentally in [4].

4. Conclusion

Nonlinear instabilities induced by oscillating voltages imposed on semiconductor devices have been observed experimentally. Studying the rich structures of such phenomena can give us a better understanding on the performance of the semiconductors. In this work, we extend the two-impurity-level model by including the time-dependent balance equation of the mean

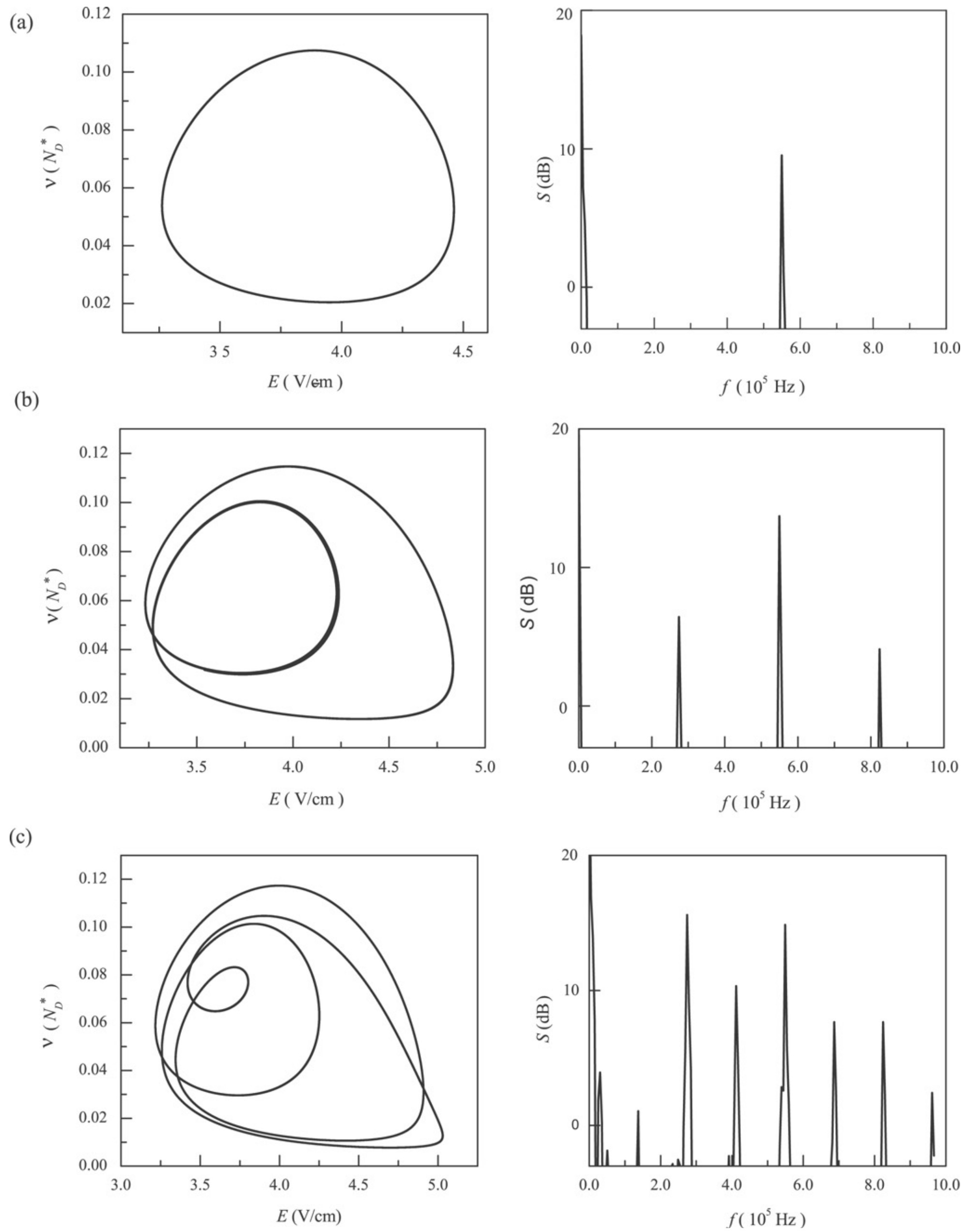

Figure 3. Left column, phase portraits of the conduction electron concentration $\nu(t)$ versus the electric field $E(t)$; right column, power spectrum $S(f)$ of $\nu(t)$ for the driving frequency $f_\mathrm{d} = 5.0 \times 10^5$ Hz and five increasing drive amplitudes: (a) $E_\mathrm{ac} = 0.8$ V cm^{-1}, (b) $E_\mathrm{ac} = 0.9$ V cm^{-1}, (c) $E_\mathrm{ac} = 0.94$ V cm^{-1}, (d) $E_\mathrm{ac} = 0.944$ V cm^{-1}, and (e) $E_\mathrm{ac} = 0.945$ V cm^{-1}.

energy per carrier to inspect theoretically the driven instability from the n-GaAs semiconductor device with the planar-type contacts as shown in figure 1 under the series connection of the ac and the dc sources. The effects from the electric field and the electron temperature variation on

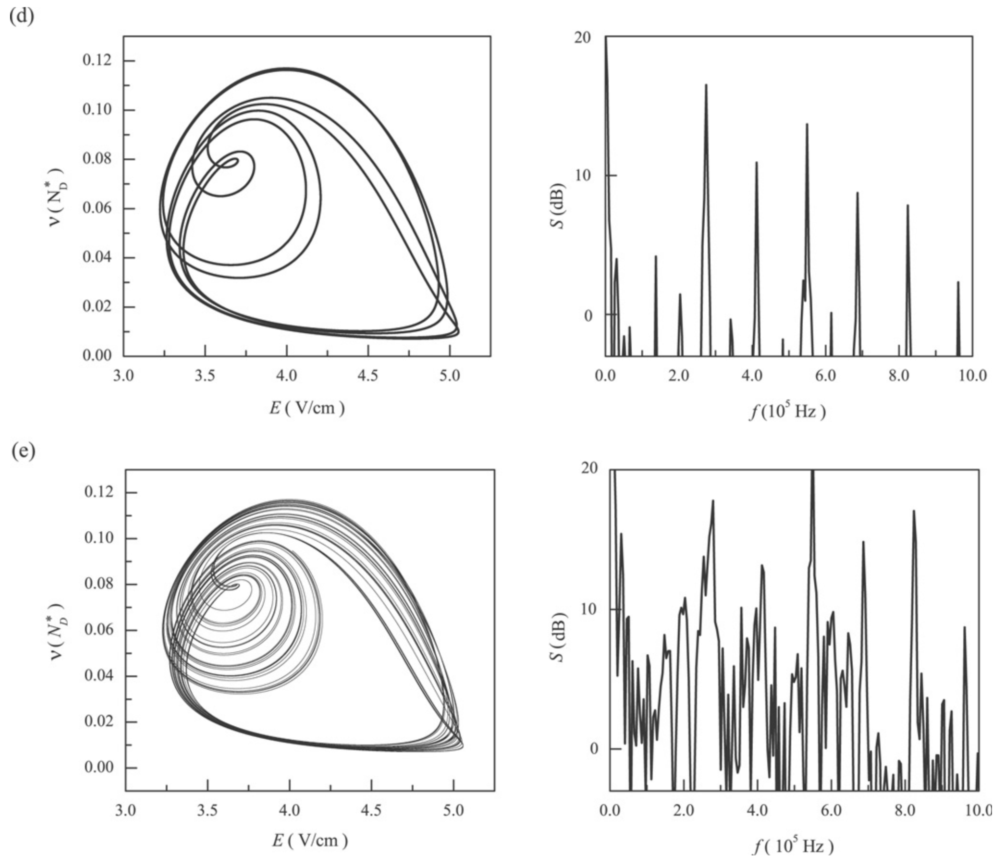

Figure 3. (Continued.)

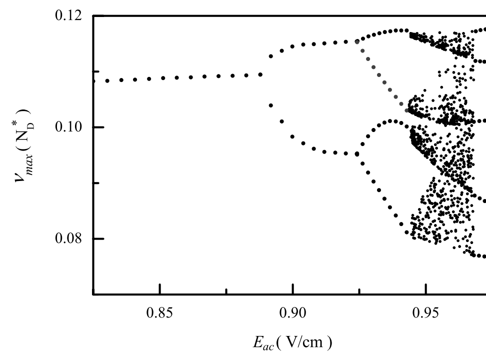

Figure 4. Bifurcation map of the conduction electron concentration maxima $\nu_{\max}$ versus the ac drive amplitude $E_{\rm ac}$, for the dc bias $E_0 = 5.599\,985$ V cm^{-1}.

the rate equations and the GR coefficients are taken into account here. Two different functions $\mu_{\rm up}$ and $\mu_{\rm lo}$ have been used to express the enhancement of the mobility on the upper branch, where $\mu_{\rm up}$ is supported by the BH formula to take into account the screen effect of the ionized-impurity scattering, and $\mu_{\rm lo}$ is retained in the empirical saturation form. To proceed with

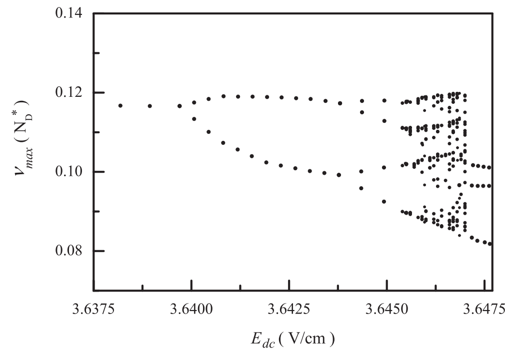

Figure 5. Bifurcation map of the conduction electron concentration maxima $\nu_{\max}$ versus the dc electric field across the sample $E_{\rm dc}$, for the ac bias amplitude $E_{\rm ac} = 0.945$ V cm^{-1} and the frequency $f_{\rm d} = 5.5 \times 10^5$ Hz.

numerical simulations, we first find the stable hysteresis loop (I–V curve) under the dc bias and the dark conditions. In order to observe chaos, we set the amplitudes of the ac voltage to be larger than the hysteresis width and appropriately bias the load line in the hysteresis region to choose the operation points which are stable without ac bias. We then solve the coupled differential equations of the GR rate equations, the energy balance equation, and the dynamic equation for the drift electric field. The numerical computations are performed under the schemes of (i) keeping the dc voltage and the ac frequency constant but gradually adjusting the ac amplitude and (ii) fixing the amplitude and the frequency of the ac source and varying the dc voltage. For both schemes, we can obtain clear current oscillating to chaos via period doubling routes. We demonstrate the results in phase portraits and their Fourier power spectra as well as bifurcation maps in details. Our results preserve the main features of experimental observations [1–4]. Aoki *et al* have used the feature that the system undergoes period-doubling bifurcations to chaos under dc + ac bias to propose novel applications such as a deterministic noise amplifier and a chaos memory device [42–44]. Our model shows a smooth period-doubling bifurcation as a function of $E_{\rm ac}$ and that of $E_{\rm dc}$, but still has some discrepancies in comparing with the experimental result, which has more complicated routes to chaos than the result of our simulation. Further detailed analysis on electronic turbulence requires progression of the spatiotemporal model simulation. We are currently heading in this direction.

Acknowledgments

The authors would like to thank Drs Tzyy-Jiann Wang, Wei-Feng Hsu, and Sheng-Kwang Hwang for their helpful comments and fruitful discussions. This work was supported in part by the National Science Council of the Republic of China under contract No NSC 95-2112-M-027-004.

References

[1] Aoki K, Kobayashi T and Yamamoto K 1982 *J. Phys. Soc. Japan* **51** 2373
[2] Aoki K, Yamamoto K and Mugibayashi N 1988 *J. Phys. Soc. Japan* **57** 26
[3] Aoki K 1992 *Semicond. Sci. Technol.* B **7** 474
[4] Aoki K and Yamamoto K 1989 *Appl. Phys.* A **48** 111
[5] Spangler J, Brandl A and Prettl W 1989 *Appl. Phys.* A **48** 143

[6] Aoki K, Kawase Y, Yamamoto K and Mugibayashi N 1990 *J. Phys. Soc. Japan* **59** 20
[7] Aoki K, Kondo T and Watanabe T 1991 *Solid State Commun.* **77** 91
[8] Aoki K and Kondo T 1991 *Phys. Lett.* A **154** 281
[9] Röhricht B, Wessely B, Peinke J, Mühlbach A, Parisi J and Huebener R P 1985 *Physica* B **134** 281
[10] Spangler J, Margull U and Prettl W 1992 *Phys. Rev.* B **45** 12137
[11] Murawski J, Schwarz G, Novak V, Prettl W and Schöll E 2005 *Angew. Math. Mech.* **85** 823
[12] Novák V, Hirschinger J, Niedernostheide F-J, Prettl W, Cukr M and Oswald J 1998 *Phys. Rev.* B **58** 13099
[13] Gaa M, Kunz R E, Schöll E, Eberle W, Hirschinger J and Prettl W 1996 *Semicond. Sci. Technol.* **11** 1646
[14] Schöll E 1987 *Nonequilibrium Phase Transitions in Semiconductors* (Berlin: Springer)
[15] Schöll E 2001 *Nonlinear Spatio-Temporal Dynamics and Chaos in Semiconductors* (Cambridge: University Press)
[16] Schöll E 1985 *Physica* B **134** 271
[17] Weispfenning M, Hoeser I, Böhm W, Prettl W and Schöll E 1985 *Phys. Rev. Lett.* **55** 754
[18] Schöll E 1986 *Slid-State Electron.* **29** 687
[19] Schöll E 1986 *Phys. Rev.* B **34** 1395
[20] Obermaier R, Böhm W, Prettl W and Dirnhofer P 1984 *Phys. Lett.* A **105** 149
[21] Schöll E, Parisi J, Röhricht B, Peinke J and Huebener R P 1987 *Phys. Lett.* A **119** 419
[22] Aoki K and Yamamoto K 1983 *Phys. Lett.* A **98** 72
[23] Hüpper G, Schöll E and Rein A 1992 *Mod. Phys. Lett.* B **6** 1001
[24] Röhricht B, Wessely B, Peinke J, Mühibach A, Parist J and Huebener R P 1985 *Physica* B **134** 281
[25] Tzeng S Y T and Cheng Y C 2003 *Phys. Rev.* B **68** 035211
[26] Tzeng S Y T and Tzeng Y 2004 *Phys. Rev.* B **70** 085208
[27] Tzeng S Y T and Tzeng Y 2005 *Phys. Rev.* B **72** 205201
[28] Teitsworth S W, Westervelt R M and Haller E E 1983 *Phys. Rev. Lett.* **51** 825
[29] Teitsworth S W and Westervelt R M 1984 *Phys. Rev. Lett.* **53** 2587
[30] Aoki K, Mugibayashi N and Yamamoto K 1986 *Phys. Scr.* T **14** 76
[31] Aoki K and Mugibayashi N 1989 *Appl. Phys.* A **48** 161
[32] Aoki K 2000 *Nonlinear Dynamics and Chaos in Semiconductors* (Bristol: Institute of Physics Publishing)
[33] Kehrer B, Quade W and Schöll E 1995 *Phys. Rev.* B **51** 7725
[34] Gaa M, Kunz R E and Schöll E 1996 *Phys. Rev.* B **53** 15971
[35] Shockley W 1961 *Solid-State Electron.* **2** 35
[36] Peinke J, Parisi J, Rössler O E and Stoop R 1992 *Encounter with Chaos* (Berlin: Springer)
[37] Schöll E 1985 *Physica* B & C **134** 271
[38] Westervelt R M and Teitsworth S W 1985 *J. Appl. Phys.* **57** 5457
[39] Seeger K 1999 *Semiconductor Physics, An Introduction* 7th edn (Berlin: Springer) p 171
[40] Aoki K 1991 *Phys. Lett.* A **152** 485
[41] Spangler J, Finger B, Wimmer C, Eberle W and Prettl W 1994 *Semicond. Sci. Technol.* **9** 373
[42] Aoki K, Matsuura A and Takahashi Y 1994 *Semicond. Sci. Technol.* **9** 607
[43] Aoki K and Yamamoto K 1992 *Proc. 21st Int. Conf. on the Physics of Semiconductors* (Singapore: World Scientific) p 261
[44] Aoki K 1993 *Proc. NATO ARW on NDR and Instabilities in 2-D Semiconductors* (New York: Plenum) p 393